An improved design for an integrated optical isolator based on nonreciprocal Mach-Zehnder interferometry

N. Bahlmann, M. Lohmeyer, M. Wallenhorst, H. Dötsch and P. Hertel
University of Osnabrück, 49069 Osnabrück, Germany

November 4, 1997

Abstract

Nonreciprocal rib waveguide structures can be used to realize integrated optical isolators. In this paper, we propose a concrete design for a Mach-Zehnder interferometer type isolator for TM modes. Just one of the arms, which are of equal length, is a nonreciprocal magneto-optic waveguide. The rest of the interferometer is reciprocal. Required fabrication tolerances are estimated, and the entire isolator is simulated by applying a finite difference beam propagation method.

1 Introduction

Magneto-optic isolators play an important role in optical communication technique. They are used to protect the semiconductor lasers from reflected light. At present only bulk isolators are available. To realize cheap integrated optical isolators, magnetic garnet films can be used. They have low absorption and high Faraday rotation in the near infrared. The Faraday rotation, which is the basis for nonreciprocal effects, can be enhanced by bismuth substitution.
Various kinds of optical isolators have been proposed by a number of researchers [1, 2, 3, 4, 5, 6]. The most promising concepts of integrated optical isolators rely on nonreciprocal Mach-Zehnder interferometry [7, 8]. The distinction between forward and backward propagation is achieved by the differential nonreciprocal phase shift (NRPS) $\Delta\beta$, the difference between the forward and backward propagation constants $\Delta\beta = \beta^{\mathrm{TM}}_{\mathrm{forw}} - \beta^{\mathrm{TM}}_{\mathrm{back}}$ of TM modes in magneto-optic waveguides [9]. In forward direction, waves propagating along both arms of the Mach-Zehnder interferometer are in phase, in backward direction a phase shift of π occurs. In former papers no concrete design for an isolator with one nonreciprocal arm was suggested. Here we present detailed design and fabrication considerations for the realization of such an isolator based on nonreciprocal Mach-Zehnder interferometry. We show how the intrinsic phase of the interferometer can be adjusted to zero in forward propagation direction. Furthermore, we simulate the new design by a finite difference beam propagation calculation.

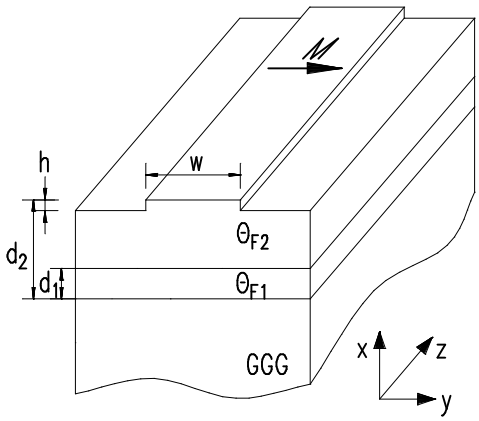

Figure 1: Basic geometry of the rib waveguide.

2 Nonreciprocal Waveguides

The following analysis is performed for the basic rib geometry sketched in Fig. 1. Mode propagation is assumed along the z axis and the magnetization $\boldsymbol{M}$ is adjusted in the film plane perpendicular to the propagation direction. Neglecting optical damping, the dielectric tensor of the magneto-optic films can be written as

$$\hat{\epsilon} = \begin{pmatrix} n^2 & 0 & \mathrm{i}\xi \\ 0 & n^2 & 0 \\ -\mathrm{i}\xi & 0 & n^2 \end{pmatrix}. \tag{2.1}$$

n is the refractive index and ξ represents the magneto-optic effect. ξ is related to the Faraday rotation Θ_F by

$$\xi \approx 2n\Theta_\mathrm{F}/k_0, \tag{2.2}$$

where k_0 is the vacuum wave number.

Using Maxwell's equations, one can derive the following partial differential equations describing quasi TE and quasi TM modes, respectively [10]:

$$(-\partial_x^2 - \partial_y^2 + \beta^2)E_y = \epsilon k_0^2 E_y \ , \tag{2.3}$$

$$(-\epsilon\partial_x\epsilon^{-1}\partial_x - \partial_y^2 + \beta^2 - \epsilon\beta(\partial_x\xi/\epsilon^2))H_y = \epsilon k_0^2 H_y \ , \tag{2.4}$$

with $\epsilon = n^2$. The TM mode equation contains a term linear in β which causes the nonreciprocal effect. TE modes propagate reciprocally in this approximation.

These equations may be solved using a finite difference [10] or a finite element method [11]. Since the term $\epsilon\beta(\partial_x\xi/\epsilon^2)$ can be regarded as a small perturbation, we first solve the unperturbed mode equation utilizing a finite element method [12]. Then perturbation theory yields

$$\Delta\beta = \frac{\iint |H_y|^2(\partial_x\xi/\epsilon^2)dxdy}{\iint \epsilon^{-1}|H_y|^2 dxdy} \tag{2.5}$$

for the differential nonreciprocal phase shift [13]. To achieve a large $|\Delta\beta|$, double layer garnet films with opposite Faraday rotation are prepared where the boundary between layers is located close to the maximum of $|H_y|^2$ [14].

To reverse the sign of the Faraday rotation from negative to positive, gallium is substituted onto the tetrahedral sites of the garnet until the magnetization of the octahedral sites

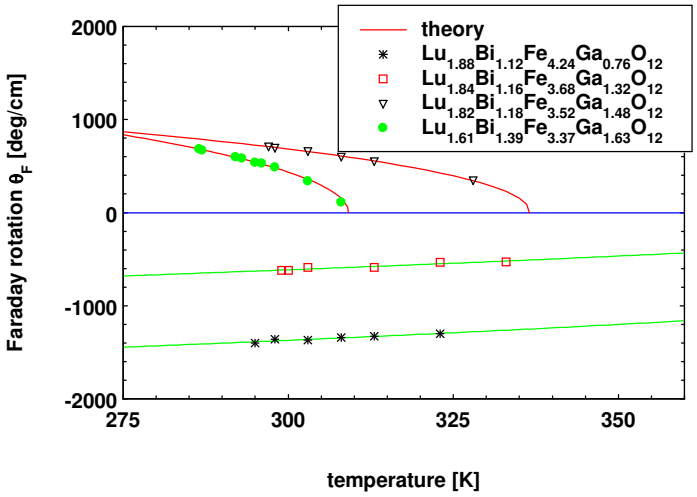

Figure 2: Temperature dependence of Θ_F for different garnet films at λ=1.3 μm. The compositions of the films are given in the legend.

dominates. Thus a compensation wall is established separating the layers with $\Theta_F^- < 0$ and $\Theta_F^+ > 0$. This procedure always results in $|\Theta_F^-| > |\Theta_F^+|$, see Ref. [14]. To achieve a large $|\Delta\beta|$ it is necessary that the layer with the larger absolute value of the Faraday rotation is the top layer. The disadvantage of this configuration is that the layer with the positive Faraday rotation shows a large temperature dependence of Θ_F as displayed in Fig. 2. This leads also to a large temperature dependence of the differential nonreciprocal phase shift. To avoid this problem we replace the layer with the positive Faraday rotation by a paramagnetic garnet layer with negligible Faraday rotation. The differential nonreciprocal phase shift of such waveguides is smaller than that of a double layer waveguide with opposite Faraday rotation, but much larger if compared with a single layer waveguide. Fig. 3 shows the calculated differential nonreciprocal phase shift for three different structures with realistic parameters. Although the maximal absolute nonreciprocal phase shift of the double layer rib waveguide (C) is 1.25 times larger than that of a double layer rib waveguide with a paramagnetic buffer layer (B), the latter waveguides should be used to realize nonreciprocal devices with small temperature dependence.

3 Nonreciprocal Mach-Zehnder interferometer

The double layer rib waveguides described above can be used to realize the nonreciprocal part of an integrated Mach-Zehnder interferometer. Auracher and Witte [7] first proposed an integrated optical isolator on the basis of a Mach-Zehnder interferometer with one nonreciprocal arm. Later Okamura et al. [8] made a proposal for a Mach-Zehnder interferometer with two nonreciprocal arms. Mizumoto et al. [15] showed a concrete design for such an isolator. A gold electrode above the waveguiding structures is used to adjust the magnetization perpendicular to the direction of propagation with opposite sign in the two branches. Because the couplers are made by magneto-optic waveguides as well, the lengths of the nonreciprocal phase shifters is not well defined.

To avoid this problem we propose a Mach-Zehnder interferometer type isolator with one nonreciprocal arm of well known length. The length of the nonreciprocal part L_{NRPS} must be chosen properly to yield a phase difference of π between the forward and backward propagating light. The basic geometry of the device is sketched in Fig. 4. First we will

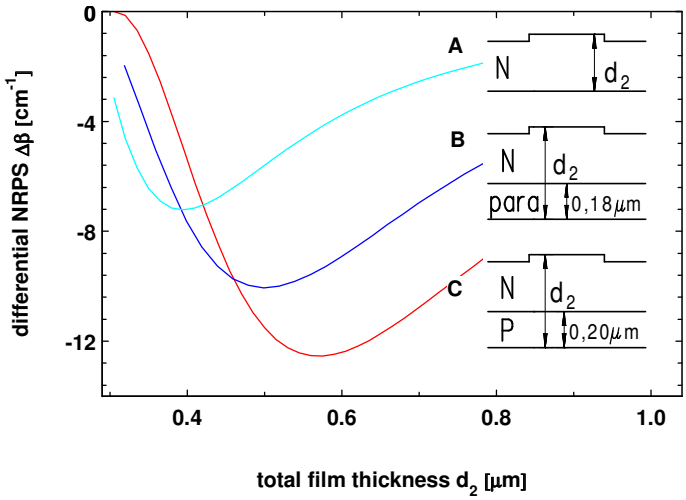

Figure 3: Calculated differential nonreciprocal phase shift (NRPS) $\Delta\beta$ for different waveguide structures at $\lambda = 1.3$ μm. The waveguide parameters of the layers denoted by N are $n = 2.33$ and $\Theta_F = -1450°/\text{cm}$, for P: $n = 2.27$ and $\Theta_F = +350°/\text{cm}$, and for para: $n = 2.20$ and $\Theta_F = 0°/\text{cm}$. The rib width w and the rib height h are 1.5 μm and 0.04 μm and the refractive indices of the substrate and cover are 1.95 and 1, respectively. The thickness of the bottom layer is chosen to yield maximum nonreciprocal phase shift.

structure the complete Mach-Zehnder interferometer in the magnetic garnet layer using an IBE (ion beam etching) technique. For monomode rib waveguides the rib height must be smaller than 40 nm at a rib width of 1.5 μm. Then the nonreciprocal part must be covered with a well defined mask, so that the top magnetic layer can be removed entirely from the reciprocal part. This region must be refilled with a nonmagnetic, dielectric material of a comparable refractive index like titanium dioxide (TiO_2). TiO_2 can be deposited by different techniques [16, 17]. The thickness of this dielectric layer must be accurately chosen, so that the propagation constant β of the reciprocal waveguide equals the propagation constant of the nonreciprocal part in forward direction β_{forw}. In this case constructive interference occurs in forward direction (A→B) if the two interferometer arms have the same length. In the backward direction (B→A) we have destructive interference.

We mention several advantages of this geometry. Because of the symmetry of the y-couplers we expect an ideal power splitting ratio of 50%. The nonreciprocal part is well defined. This leads to a fixed nonreciprocal phase shift of π. No electrodes or permanent magnets on top of the waveguides are needed to reverse the direction of the magnetization between the arms. It is sufficient to magnetize the nonreciprocal part by an external bias magnetic field. For the same reason the gap between the two interferometer arms can be smaller (as compared with the interferometer with two nonreciprocal arms). Therefore, the length of the total device decreases (the y-couplers will be shorter). Since the propagation constants in the reciprocal and nonreciprocal waveguides are equal no additional reflections occur.

There are also some problems which are typical for our design concept. Since we use only one nonreciprocal arm, the length of the interferometer arms is twice as long as that of a device with two nonreciprocal arms. Furthermore, the dielectric material for the reciprocal part must have a comparable optical absorption, otherwise the intensities in the different arms are not equal and destructive interference is incomplete.

Another problem is to adjust the intrinsic phase of the interferometer. With the optimal

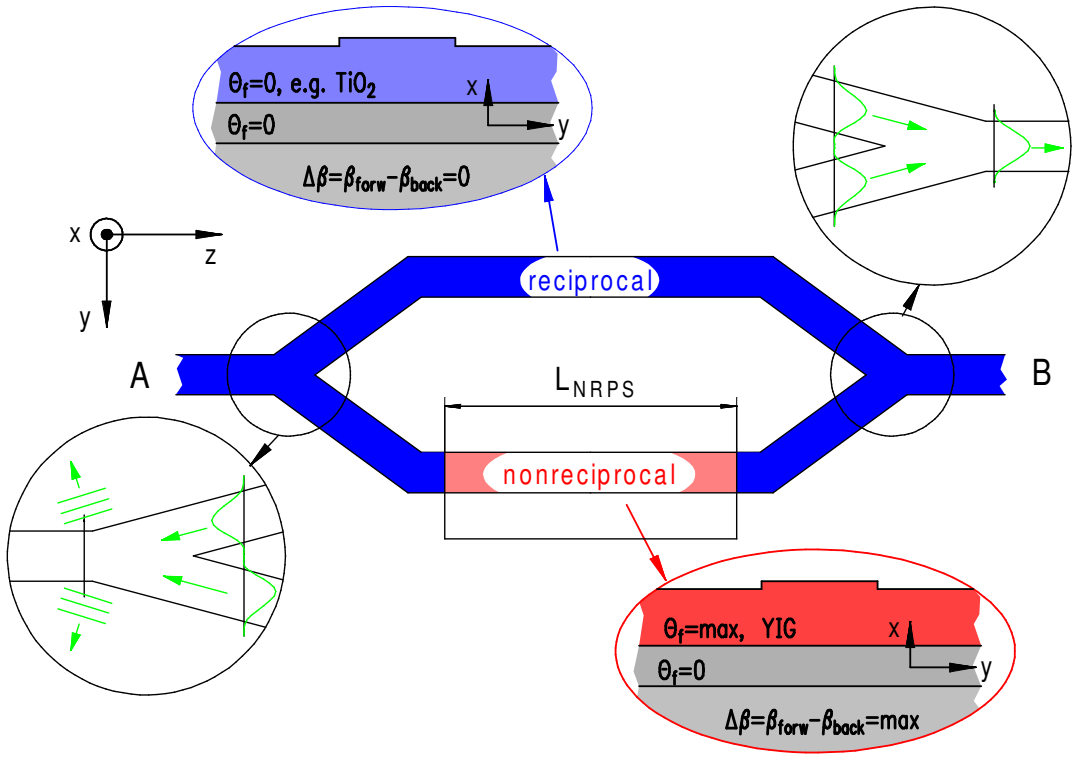

Figure 4: Basic geometry of the nonreciprocal Mach-Zehnder interferometer.

film parameters (see Fig. 3) we achieve a maximal differential nonreciprocal phase shift of 10.05 cm^{-1} which results in an arm length of $L_{\mathrm{NRPS}} = \pi/\Delta\beta = 3123\mu\mathrm{m}$. At this distance a thickness deviation of about 1 nm of the reciprocal arm leads to an additional phase of more than 3π (see Fig. 5). Since a phase difference accuracy of a few degrees is necessary for the desired isolation ratio it is impossible to control the film thickness of the dielectric layer during the growth process with the required accuracy. Therefore, the intrinsic phase must be adjusted in a further process step. This can be done by local annealing [18] or by stepwise etching of one waveguide [19]. The requirements for the tuning are discussed in chapter 4.

4 Fabrication Tolerances

In order to calculate the fabrication tolerances for the isolator structures we first have to describe the desired device specifications. The integrated isolator should at least fulfill the specifications of comparable bulk devices and microisolators. The insertion loss, which is the relation between the input and output power in forward direction, should be smaller than 1.5 dB, and the isolation ratio, the relation between the output power in forward and backward direction, must achieve at least 30 dB. Furthermore, it should operate in a temperature and wavelength range as large as possible.

To determine the forward loss and the backward attenuation of the Mach-Zehnder isolator we use the following expression [20]:

$$P_{\mathrm{out}} = \frac{P_{\mathrm{in}}}{2} K \mathrm{e}^{-\alpha L} (1 + 2\sqrt{\bar{\alpha}(1-\bar{\alpha})}\cos\Phi). \tag{4.1}$$

P_{in} and P_{out} denote the input and output power, respectively. The damping of the waveguides is α and the length is L. K describes additional losses which are caused e. g. by

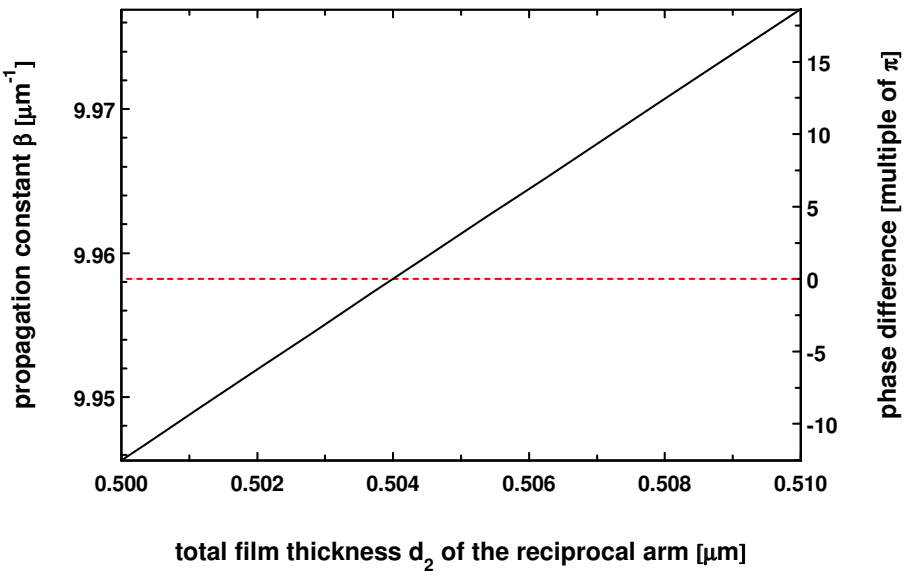

Figure 5: Calculated propagation constant β of the reciprocal arm (left axis) and the phase difference between the reciprocal and nonreciprocal arm in forward direction at an arm length of 3123μm (right axis). For a film thickness of $d_2 = 0.504\mu$m both arms are in phase.

the y-couplers. The splitting ratio of the y-couplers is described by $\bar{\alpha}$ (1/2 for ideal couplers). The most important factor is the phase difference Φ between the arms. In forward direction it should be zero, in backward direction π.

The insertion loss depends mainly on the losses of the y-couplers and on the waveguide absorption multiplied with the device length. The loss of the couplers is typically smaller than 0.2 dB for a half branching angle $< 1°$. It follows, that αL must be smaller than 1.1 dB. For a typical device length of 5 mm the waveguide damping must be smaller than 2.2 dB/cm.

Furthermore, it is important that there is no phase difference in forward direction. As described in the previous chapter, it is necessary to tune the intrinsic phase of the interferometer in a postfabrication process. One tuning possibility is to change the propagation constant on a short part of one arm by reducing the waveguide thickness. If we reduce the thickness by about 1 nm on a length of 5 μm, the phase is changed by about 0.9 degree (see Fig. 5). Since we can estimate the intrinsic phase from the relation between the output power in forward and backward direction it is possible to tune the interferometer within a few etching steps.

If the intrinsic phase of the interferometer in forward direction is adjusted to zero, the isolation ratio depends chiefly on the nonreciprocal phase shift between forward and backward direction. Another important factor is the splitting ratio of the y-couplers. Since waveguide or radiation losses occur as well in forward as in backward direction they do not influence the isolation ratio. Using eq. (4.1) we can calculate the isolation ratio $P_{\mathrm{forw}}/P_{\mathrm{back}}$ for different nonreciprocal phase shifts and splitting ratios of the Mach-Zehnder interferometer. Fig. 6 shows the results if the intrinsic phase is assumed to be zero. In order to achieve an isolation of at least 30 dB, the nonreciprocal phase shift must be in the range of $180° \pm 3°$ if the splitting ratio $\bar{\alpha}$ of the y-couplers lies between 0.48 and 0.52 which are typical values for power splitters. The length of the nonreciprocal part can be fabricated with a precision of at least 5 μm. Therefore, the deviation of the differential nonreciprocal phase shift must be smaller than 0.15 cm^{-1} to achieve a phase deviation smaller than 3°.

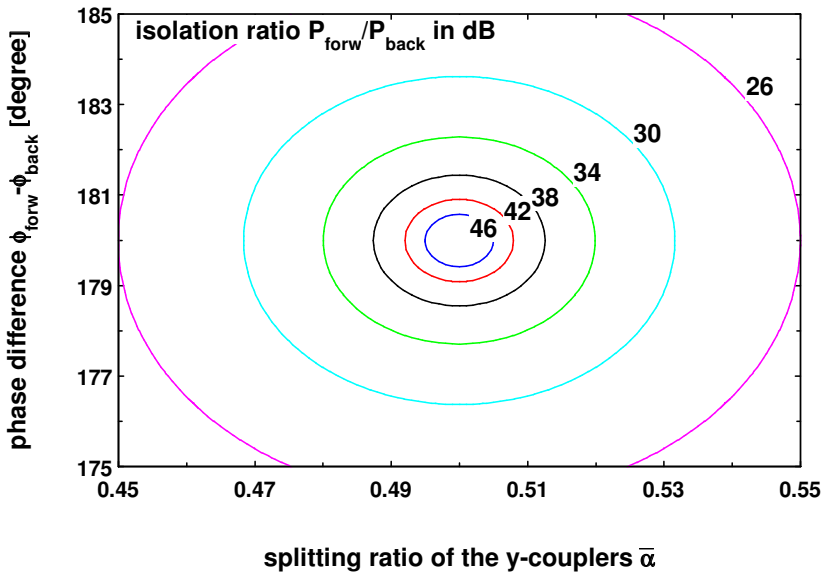

Figure 6: Calculated isolation ratio $P_{\text{forw}}/P_{\text{back}}$ for a nonreciprocal Mach-Zehnder interferometer. The intrinsic phase is assumed to be zero.

This is equivalent to a thickness variation of less than 0.03 μm (see Fig. 3). These spatial requirements can be satisfied if the garnet films are handled with modern lithography and clean room techniques. The biggest problem is the tuning of the intrinsic phase.

The temperature dependence of the differential nonreciprocal phase shift can be determined with the values for the Faraday rotation given in Fig. 2. The curve in Fig. 7 shows the calculated differential and integral nonreciprocal phase shift in the temperature range 273-323 K. At room temperature the nonreciprocal phase shift is 180°, as required. But only in the temperature range from approximately 290 K to 305 K the condition for 30 dB isolation (see Fig. 6) is fulfilled. Therefore, we have to reduce the temperature dependence of the Faraday rotation or we have to find waveguide structures with compensated temperature dependence.

5 Finite Difference Beam Propagation Simulation

In order to simulate the behaviour of realistic nonreciprocal devices like Mach-Zehnder interferometers or nonreciprocal couplers, we employ a finite difference beam propagation method for nonreciprocal three dimensional structures (two dimensional cross section, one propagation dimension). Different beam propagation techniques for reciprocal waveguides were introduced by a number of researchers [21, 22, 23]. Erdmann et. al [24] introduced a BPM method for planar magneto-optic waveguides.

The complexity of our problem can be reduced with the effective index approximation [25] (see Fig. 8). The effective indices ($n_{\text{eff}} = \beta/k_0$) for the TM modes of our waveguides must be calculated with equation 2.4, if the partial derivatives in y-direction are neglected. Because of the term linear in β we obtain different effective indices for forward and backward propagation in the magneto-optic waveguide.

The following calculations are performed with such effective indices. Since we have different indices for forward and backward direction we have to carry out the BPM calculation twice.

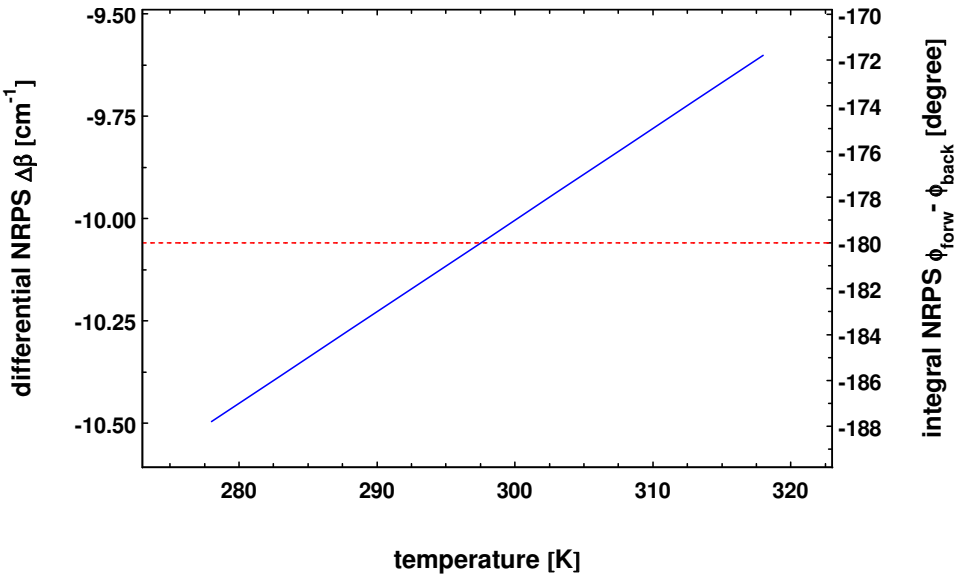

Figure 7: Calculated temperature dependence of the differential and integral nonreciprocal phase shift for the waveguide denoted with B in Fig. 3. The integral nonreciprocal phase shift is calculated for L_{NRPS}=3123 μm. The temperature dependence of the Faraday rotation is shown in Fig. 2.

In paraxial approximation one obtains the Fresnel equation [22]

$$2\mathrm{i}k_0 n_{\mathrm{ref}} \frac{\partial E_x}{\partial z} = \frac{\partial^2 E_x}{\partial y^2} + k_0^2[n_{\mathrm{eff}}^2(y) - n_{\mathrm{ref}}^2]E_x \tag{5.1}$$

for the dominating electric field component E_x of the TM mode. The reference index n_{ref} is supplied by a calculation without magneto-optic effect.

The Fresnel equation is solved with a finite difference Crank-Nicolson procedure. In order to suppress reflections from the boundaries, transparent boundary conditions are implemented [26].

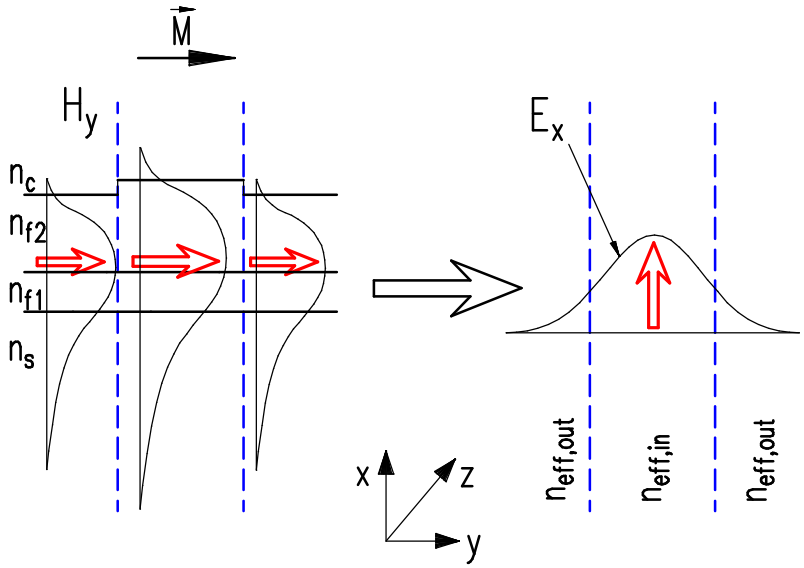

Figure 8: Symbolic presentation of the effective index approximation for TM modes.

6 Numerical Results

In this section we present results of the BPM calculations. Fig. 9 shows the calculated fields for the forward and backward direction. The geometry parameters of the Mach-Zehnder interferometer are given in the figure caption. The total power in the computational window is plotted in Fig. 10. Almost 97 % of the input light passes the isolator in forward direction, but only 0.1 % in backward direction, the rest leaving the device in lateral direction. This amounts to an isolation exceeding 30 dB.

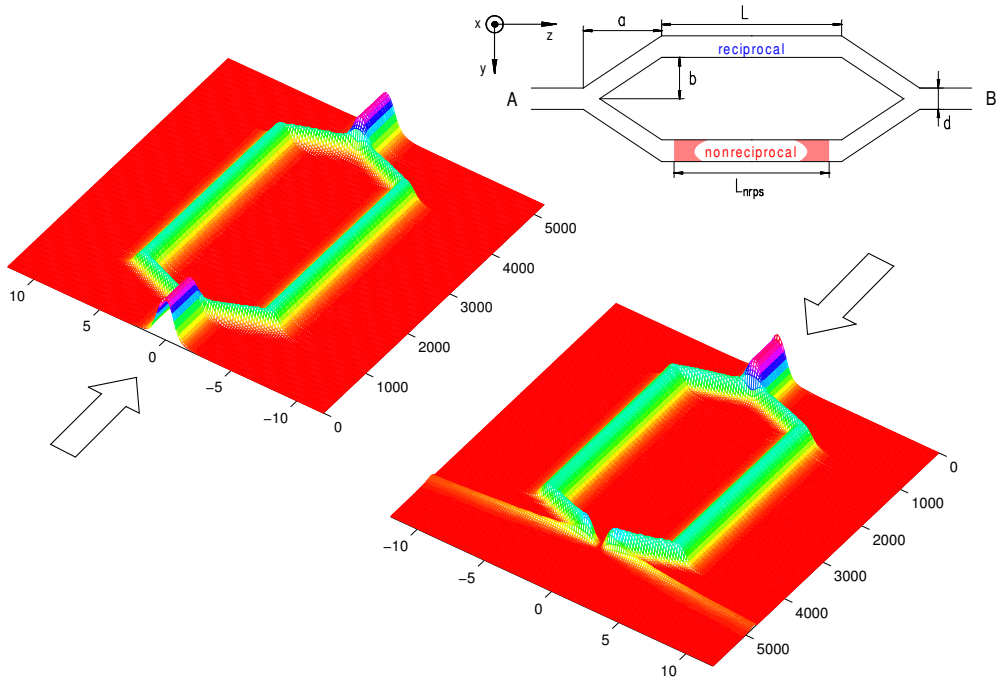

Figure 9: BPM simulation of the Mach-Zehnder interferometer. For the nonreciprocal part we use the layer configuration (B) from Fig. 3 at a film thickness of 504 nm. ($a = 400$ μm, $b = 4$ μm, $d = 1.5$ μm, $L = 3250$ μm, $L_{\mathrm{NRPS}} = 3123$ μm).

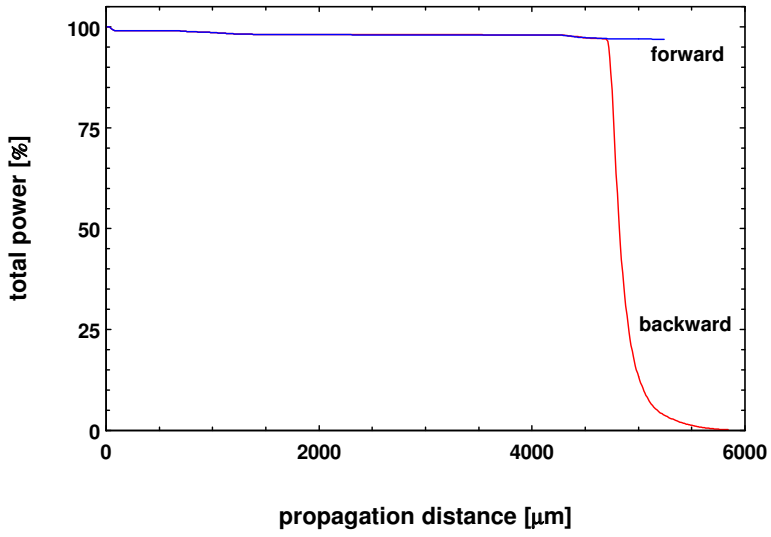

Figure 10: The total power in the computational window for the simulation in Fig. 9. Up to the second y-coupler the total power is equal for forward and backward direction.

In order to control the accuracy of the BPM calculations, we compute the output power in backward direction for different lengths of the nonreciprocal phase shifter L_{NRPS} and compare the results with equation (4.1). The intrinsic phase in forward direction is assumed to be zero. Fig. 11 shows good agreement between the two different calculations.

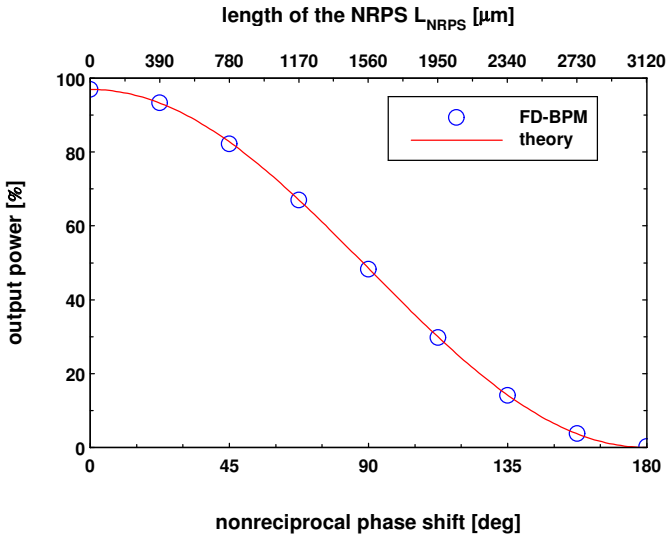

Figure 11: Total power in the computational window in backward direction for different lengths of the nonreciprocal part. The nonreciprocal phase shift is $\Delta\beta \cdot L_{\mathrm{NRPS}}$. The solid line is calculated with eq. (4.1).

7 Summary

We demonstrate that double layer rib waveguides with one paramagnetic and one magneto-optic layer are a good choice to realize nonreciprocal Mach-Zehnder interferometer devices. They show a large differential nonreciprocal phase shift and low temperature dependence. We propose an improved design for a nonreciprocal Mach-Zehnder interferometer isolator which utilizes such waveguides. An outstanding feature of our concept is that the nonreciprocal part of the interferometer is well defined. This leads to a well known nonreciprocal phase shift. Low forward losses and large isolation will be achieved if the intrinsic phase of the interferometer is tuned to zero in a postfabrication process. Simple BPM calculations with different effective refractive indices for forward and backward direction work well to simulate light propagation in the device.

Acknowledgements

We gratefully acknowledge financial support by Deutsche Forschungsgemeinschaft, Sonderforschungsbereich 225.

References

[1] R. WOLFE, J. DILLON JR., R. A. LIEBERMAN and V. J. FRATELLO, *Applied Physics Letters* **57** (1990) 960.

[2] K. ANDO, T. OKOSHI and N. KOSHIZUKA, *Applied Physics Letters* **53** (1988) 4.

[3] T. MIZUMOTO, Y. KAWAOKA and Y. NAITO, *The Transactions of the IECE of Japan* **E 69** (1986) 968.

[4] H. HEMME, H. DÖTSCH and P. HERTEL, *Applied Optics* **29** (1990) 2741.

[5] S. YAMAMOTO, Y. OKAMURA and T. MAKIMOTO, *IEEE Journal of Quantum Electronics* **QE-12** (1976) 764.

[6] T. SHINTAKU, *Applied Physics Letters* **66** (1995) 2789.

[7] F. AURACHER and H. WITTE, *Optics Communications* **13** (1975) 435.

[8] Y. OKAMURA, T. NEGAMI and S. YAMAMOTO, *Applied Optics* **23** (1984) 1886.

[9] S. YAMAMOTO and T. MAKIMOTO, *Journal of Applied Optics* **45** (1974) 882.

[10] A. ERDMANN, M. SHAMONIN, P. HERTEL and H. DÖTSCH, *Optics Communications* **102** (1993) 25.

[11] M. KOSHIBA and X. ZHUANG, *Journal of Lightwave Technology* **11** (1993) 1453.

[12] N. MABAYA, P. LAGASSE and P. VANDENBULCKE, *IEEE Transactions on Microwave Theory and Techniques* **MTT-29** (1981) 600.

[13] M. SHAMONIN and P. HERTEL, *Applied Optics* **33** (1994) 6415.

[14] M. WALLENHORST, M. NIEMÖLLER, H. DÖTSCH, P. HERTEL, R. GERHARDT and B. GATHER, *Journal of Applied Physics* **77** (1995) 2902.

[15] T. MIZUMOTO, S. MASHIMO, T. IDA and Y. NAITO, *IEEE Transactions on Magnetics* **29** (1993) 3417.

[16] P. LÖBL, M. HUPPERTZ and D. MERGEL, *Thin Solid Films* **251** (1994) 72.

[17] J. P. BENNETT, E. PELLETIER, G. ALBRAND, J. P. BORGOGNO, B. LAZARIDES, C. K. CARNIGLIA, R. A. SCHMELL, T. H. ALLEN, T. TUTTLE-HART, K. H. GUENTHER and A. SAXER, *Applied Optics* **28** (1989) 3303.

[18] M. J. AHMED and L. YOUNG, *Applied Optics* **22** (1983) 4082.

[19] R. WOLFE, R. A. LIEBERMAN, V. J. FRATELLO, R. E. SCOTTI and N. KOPYLOV, *Applied Physics Letters* **56** (1989) 426.

[20] W. KARTHE and R. MÜLLER, *Integrierte Optik.* Leipzig: Akademische Verlagsgesellschaft Geest & Portig, (1991).

[21] M. D. FEIT and J. A. FLECK JR., *Applied Optics* **17** (1978) 3990.

[22] Y. CHUNG and N. DAGLI, *IEEE Journal of Quantum Electronics* **26** (1990) 1335.

[23] H. J. W. M. HOEKSTRA, *Optical and Quantum Electronics* **29** (1997) 157.

[24] A. ERDMANN and HERTEL, *IEEE Journal of Quantum Electronics* **31** (1995) 1510.

[25] G. B. HOCKER and W. K. BURNS, *Applied Optics* **16** (1977) 113.

[26] G. R. HADLEY, *Optics Letters* **16** (1991) 624.